A ground-based multisensor cloud phase classifier

Matthew D. Shupe[1,2]

Received 14 June 2007; revised 21 August 2007; accepted 12 October 2007; published 22 November 2007.

[1] A method for classifying cloud phase from a suite of ground-based sensors is outlined. The method exploits the complementary strengths of cloud radar, depolarization lidar, microwave radiometer, and temperature soundings to classify clouds observed in the vertical column as ice, snow, mixed-phase, liquid, drizzle, rain, or aerosol. Although the classification has been specifically designed for observations of Arctic clouds, the general framework is applicable to other locations with minor modifications. An example classification demonstrates the application to actual measurements. **Citation:** Shupe, M. D. (2007), A ground-based multisensor cloud phase classifier, *Geophys. Res. Lett.*, *34*, L22809, doi:10.1029/2007GL031008.

1. Introduction

[2] Cloud phase identification is a necessary prerequisite to performing cloud property retrievals from remote sensor measurements. Most retrieval algorithms are specifically developed and tuned for clouds of a particular phase and type. Thus a cloud phase classifier is a crucial component to any operational algorithm for deriving cloud properties at all times and heights above ground-based atmospheric observatories, such as those associated with the DOE Atmospheric Radiation Measurement (ARM) and NOAA Study of Environmental Arctic Change (SEARCH) Programs. For the ARM program in particular a major programmatic objective is to compute accurate radiative heating rate profiles above its ARM Climate Research Facilities (ACRF). Such an endeavor is only possible with a reliable cloud microphysics product which relies on a robust cloud phase classification algorithm.

[3] There have been a number of cloud classification methods proposed using satellite measurements based on a variety of sensors and classification frameworks [*Welch et al.*, 1992; *Tovinkere et al.*, 1993; *Luo et al.*, 1995; *Rossow and Schiffer*, 1999; *Hu et al.*, 2001]. To a lesser degree, ground-based classification algorithms have been explored. In particular, methods using pyranometers [*Duchon and O'Malley*, 1999], spectral infrared interferometers [*Turner et al.*, 2003], and combined active and passive sensors [*Wang and Sassen*, 2001] have been suggested. Classification methods are based on neural networks [*Miller and Emery*, 1997; *Bankert*, 1994], fuzzy grade-of-membership systems [*Baum et al.*, 1997; *Shao*, 2000, *Talbot et al.*, 1999] and pattern recognition systems [*Ebert*, 1987]. Others are based on crisp, or fixed, threshholds between various parameters such as optical depth and cloud top pressure/temperature [*Rossow and Schiffer*, 1999]. Most methods are oriented towards a classification of meteorological cloud types [*Bankert*, 1994; *Ebert*, 1987; *Rossow and Schiffer*, 1999; *Wang and Sassen*, 2001] such as cumulus, stratus, or altostratus, although such classifications are of limited use for the subsequent application of cloud property retrievals.

[4] Here, a method is presented to classify cloud hydrometeor phase in the vertical column above intensive Arctic atmospheric observatories, such as the ARM and SEARCH sites, from a set of key measurements. The classifications are not meteorological in nature, but rather are specifically tailored to determine the vertical distribution of hydrometeor phase to facilitate subsequent phase-appropriate cloud microphysics retrievals. Furthermore, this type of classification has application towards the assessment of model simulations, where condensate is partitioned by phase, not by meteorological cloud type. The classes considered here include: liquid, drizzle, liquid+drizzle, rain, ice, snow, mixed-phase, and aerosol (defined in Table 1). This classification algorithm represents the manifestation of a manual cloud classification based on a combination of sensors [*Shupe et al.*, 2005] into a consistent, rule-based framework. While many of the rules, or thresholds, employed in the algorithm are based on physical principles and/or previous studies, some have been subjectively tuned based on extensive experience with seven years of multisensor observations to produce realistic, self-consistent classifications.

2. Instruments and Measurements

[5] Necessary measurements for the cloud phase classifier include those from depolarization lidar, cloud radar, microwave radiometer, and radiosondes. While other instruments can contribute further insight into the characterization of cloud phase, these four provide a sufficient level of information. A multisensor approach is necessary in cloud classification since no one instrument can unambiguously classify cloud phase for all clouds at a given site under all

Table 1. Cloud Phase Type Classes

Class	Description
Ice	Only cloud ice particles
Snow	Only snow particles (defined based on a reflectivity threshold which is related to particle size)
Mixed-phase	Cloud liquid droplets and cloud ice particles in the same volume
Liquid	Only cloud liquid droplets
Liquid+drizzle	Cloud liquid droplets and drizzle drops in the same volume
Drizzle	Only drizzle drops (defined based on a reflectivity threshold which is related to drop size)
Rain	Only rain drops (defined based on a Doppler velocity threshold which is related to drop size)
Aerosol	Only aerosol or haze particles but no cloud particles

[1]Cooperative Institute for Research in Environmental Science, University of Colorado, Boulder, Colorado, USA.
[2]NOAA Earth System Research Laboratory, Boulder, Colorado, USA.

0094-8276/07/2007GL031008$05.00

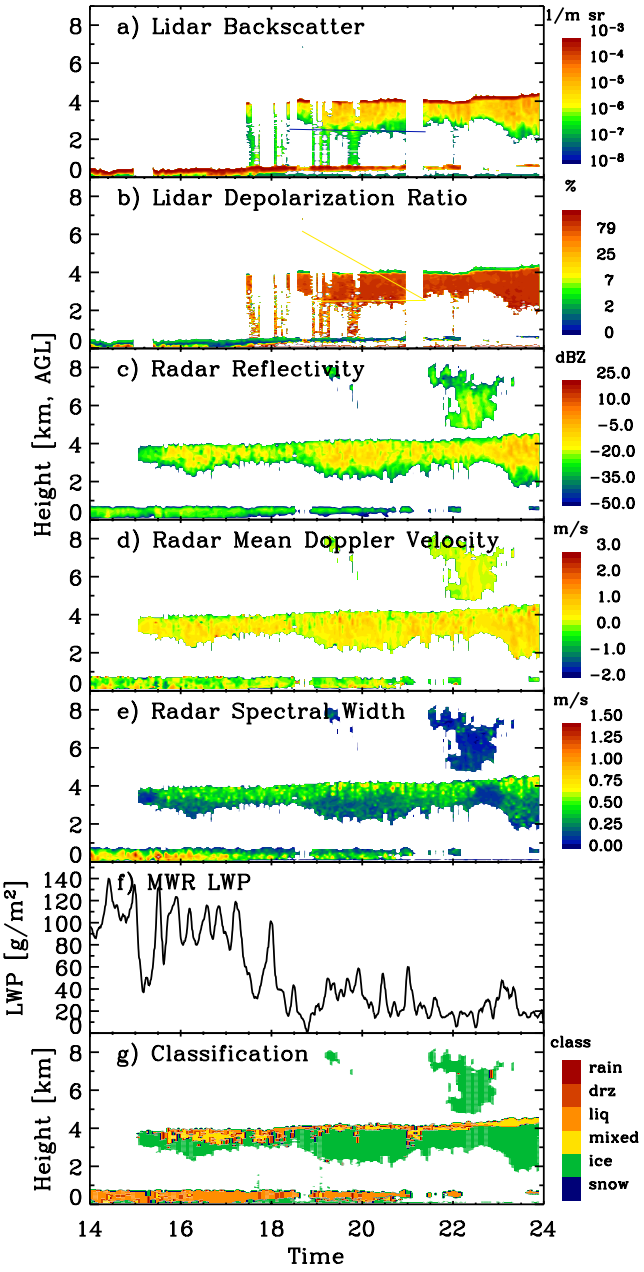

Figure 1. Case study example from 10 September 2006 at the NOAA SEARCH atmospheric observatory of (a) lidar backscatter, (b) lidar depolarization ratio, (c) radar reflectivity, (d) radar mean Doppler velocity, (e) radar Doppler spectrum width, (f) microwave radiometer-derived liquid water path, and (g) the resulting multisensor classification mask.

conditions. These basic sensors nicely complement each other in order to accomplish a generalized classification for all cloud phase types.

[6] Depolarization lidars, such as the High Spectral Resolution Lidar [*Eloranta*, 2005] or micropulse lidar [*Campbell et al.*, 2002], measure backscatter intensity (β) and depolarization ratio (δ), the combination of which results in a robust hydrometeor phase classification for nonocculted volumes. Lidar measurements are particularly useful for identifying the lower boundaries of clouds, and especially the base of cloud liquid layers. Visible wavelength lidars, however, suffer from attenuation in optically thick clouds, which often precludes observation of the full vertical atmospheric column. Furthermore, in some cases containing both large, precipitation-size particles (ice, drizzle, or rain) and numerous, small liquid cloud droplets, the stronger signal from cloud droplets may prevent the coincident identification of the larger particles.

[7] Cloud radars operating near 35- or 94-GHz, such as the Millimeter Cloud Radar (MMCR) [*Moran et al.*, 1998], provide measurements of the Doppler spectrum, and its first three moments, the reflectivity (Z_e), mean Doppler velocity (V_D), and Doppler spectrum width (W_D). Under most conditions, except for heavy rain, attenuation is minimal such that cloud radars sense cloudiness throughout the full atmospheric column. However, since reflectivity is proportional to the sixth power of the particle size, radar signals are dominated by the largest particles in a volume and thus have a lower sensitivity than lidars to the smallest particles. Radars may therefore miss some cloud fringes or tenuous cloud layers that contain small particles. Moreover, it is difficult, based on reflectivity alone, to distinguish ice clouds from mixed-phase clouds, in which ice particles are typically larger than liquid droplets and thus dominate the radar signal. Some signatures for making this distinction, however, may be available from mean Doppler velocity and/or Doppler spectrum width fields [e.g., *Shupe et al.*, 2004, 2006].

[8] Estimates of column-integrated liquid water path (LWP) are available from multichannel microwave radiometer (MWR) [*Liljegren et al.*, 2001; *Turner et al.*, 2007], and spectral infrared retrievals [*Turner*, 2007], among others. A positive LWP indicates liquid water, in some form, in the vertical atmospheric column; however, it does not vertically distribute that liquid water. LWP retrievals from MWR have an uncertainty of ~25 g/m^2 [*Westwater et al.*, 2001], which places a great deal of uncertainty on liquid water identification in clouds with low liquid water amounts. This shortcoming can be improved upon by employing the latest absorption models [e.g., *Turner et al.*, 2007], by combining infrared and microwave measurements [*Turner*, 2007], and/or by adding higher-frequency channels to the retrieval [*Crewell and Lohnert*, 2003].

[9] Temperature (T) soundings also provide crucial supporting information under certain circumstances. In particular, the −40°C homogeneous freezing and 0°C melting temperatures impart unambiguous constraints on the classification. However, over the range of −40 to 0°C, most cloud phases can exist. Measurements from an infrared thermometer, although not necessary, could provide an additional constraint on cloud base temperature for the classification.

3. Classification

[10] To illustrate the classification algorithm, a sampling of measurements from a case study on 10 September 2006 at the NOAA SEARCH site in Eureka, Canada (80.00°N, 85.81°W) is used (Figure 1), resulting in the classification mask in Figure 1g. This case contains three levels of cloudiness – low (<1 km), mid-level (2–4.5 km), and high (>4.5 km). The basic steps to the classification are outlined

Table 2. General Steps to the Classification Process

Step	Application	Details
1. Lidar mask	Lidar-viewed pixels	Figure 2a provides liquid, ice, aerosol classes
2. Modify lidar mask w/radar	Lidar-viewed pixels	Add mixed-phase, drizzle, snow classes
3. Precip mask w/radar and T	All pixels	$Z_e > 5$ dBZ & $T < 0°C$ = snow
		$Z_e > 5$ dBZ & $T > 0°C$ = rain
		$V_D > 2.5$ m/s & $T > 0°C$ = rain
4. Complete mask	Pixels not viewed by lidar	Figure 2, including lidar occultation layer classification
5. Absolute T rules	All pixels	$T < -40°C$ = ice
		$T > 0°C$ = [liquid, drizzle, rain]
6. LWP constraint	All columns of pixels	If LWP ≤ 0 g/m^2, then liquid pixels to ice
		If LWP $> 25^a$ g/m^2, then find liquid layer
7. Homogenize	All pixels	7×7 surrounding pixel box
		a)>35 clear pixels in box: pixel = clear
		b)>7 pixels of given type in box: no change
		c)$\leq$7 pixels of given type in box: change to dominant type
		d) Additional rules

[a]The value should be the uncertainty of the specific LWP estimate.

in Table 2 and described here in order. Order is important because some classifications rely upon cumulative information from multiple sensors.

[11] An initial classification is made from lidar measurements using the scheme in Figure 2a where all pixels observed by the lidar are classified as liquid, ice, or aerosol. Cloud liquid is identified by high lidar backscatter and low depolarization ratio [e.g., *Sassen*, 1984; *Intrieri et al.*, 2002], as are present in both the low-level cloud layer and at the top of the mid-level cloud near 4 km in Figures 1a and 1b. High backscatter is due to the high total surface area associated with typical populations of cloud droplets, which are small and exist in relatively high concentrations. In addition, spherical particles, which are typically liquid, do not significantly depolarize the lidar beam, resulting in very small depolarization ratios (<0.1). On the contrary, nonspherical ice crystals, which are usually larger than liquid droplets and occur in smaller concentrations, highly depolarize the lidar signal, and often have less backscatter than water droplets. By these criteria (Figure 2a), ice is indicated below about 4 km in the mid-level cloud layer and near the surface below the low-level cloud layer in Figures 1a and 1b.

[12] The lidar classification is modified in step 2 based on additional information from radar. If the lidar identifies a time-height pixel as aerosol but the radar has a measurable reflectivity, the pixel is reclassified as a cloud, since cloud radars cannot observe aerosol-size particles. In addition, if pixels are identified by the lidar to be liquid, but the radar reflectivity or mean Doppler velocity are larger than the expected ranges for liquid droplets only [$Z_e > -17$ dBZ [*Frisch et al.*, 1995] or $V_D > 1$ m/s], the pixel is reclassified as liquid+drizzle ($T > 0°C$) or mixed-phase ($T < 0°C$). A reclassification from liquid to mixed-phase was necessary in some regions near the top of the mid-level cloud in this case (i.e., 2300–2400) as a result of high reflectivity (Figure 1c).

[13] The radar observations are then used to identify periods of unambiguous, strong precipitation (step 3 in Table 2). Based on comparisons between radar observations and surface precipitation measurements, all pixels with $Z_e >$ 5 dBZ are classified as snow ($T < 0°C$) or rain ($T > 0°C$). All above-freezing pixels with $V_D > 2.5$ m/s are classified as rain, since no other Arctic hydrometeors fall at those high speeds. These criteria are applied to all pixels, including modifying those that have already been initially classified by the lidar.

[14] In step 4, since the lidar beam is occulted by optically thick cloud layers but the radar is usually not significantly attenuated, the information from the radar, augmented by radiosondes, completes the classification above the level of lidar occultation (e.g., above 0.5 km prior to 1800 and above 4.2 km after 1800 in Figure 1). Pixels at temperatures above freezing can only be a non-frozen class, and are distinguished by reflectivity and velocity thresholds (Figure 2b). At temperatures below freezing, more classifications are possible and the Doppler spectrum width is utilized. The spectrum width is generally wider when there are multiple phases or when turbulence or wind shear is significant, whereas narrower spectrum widths are most often associated with a single phase of hydrometeors under quiet conditions. For narrow widths ($W_D <$ 0.4 m/s), snow is distinguished from cloud ice by high Z_e (Figure 2d), resulting in an ice classification for the upper-level cloud observed from 2200–2300. When $W_D > 0.4$ m/s, mixed-phase clouds are characterized by higher Z_e and V_D than liquid-only clouds because they contain larger particles (Figure 2c). The mid-level cloud from 1500–1800, which is not observed by lidar, demonstrates this type of classification based on radar and temperature alone.

[15] The requirement that liquid-only cloud layers have a relatively wide spectrum width is based on experience with multisensor observations of Arctic clouds, but may misidentify some non-turbulent liquid layers that have narrow spectrum widths as ice. Furthermore, there are some cases where the spectrum width threshold may suggest mixed-phase conditions when only ice is present, which may be the case for portions of the mid-level cloud classification during 1500–1800. While it is sometimes difficult for the radar to accurately determine the thickness of mixed-phase layers in the absence of lidar measurements, the ability of the radar to identify mixed-phase layers at all is of great importance when lidar measurements are obscured.

[16] An additional component of step 4 considers clouds that are immediately above the location of lidar occultation. Occultation of the lidar signal typically occurs within a liquid layer, suggesting that cloud liquid extends above the

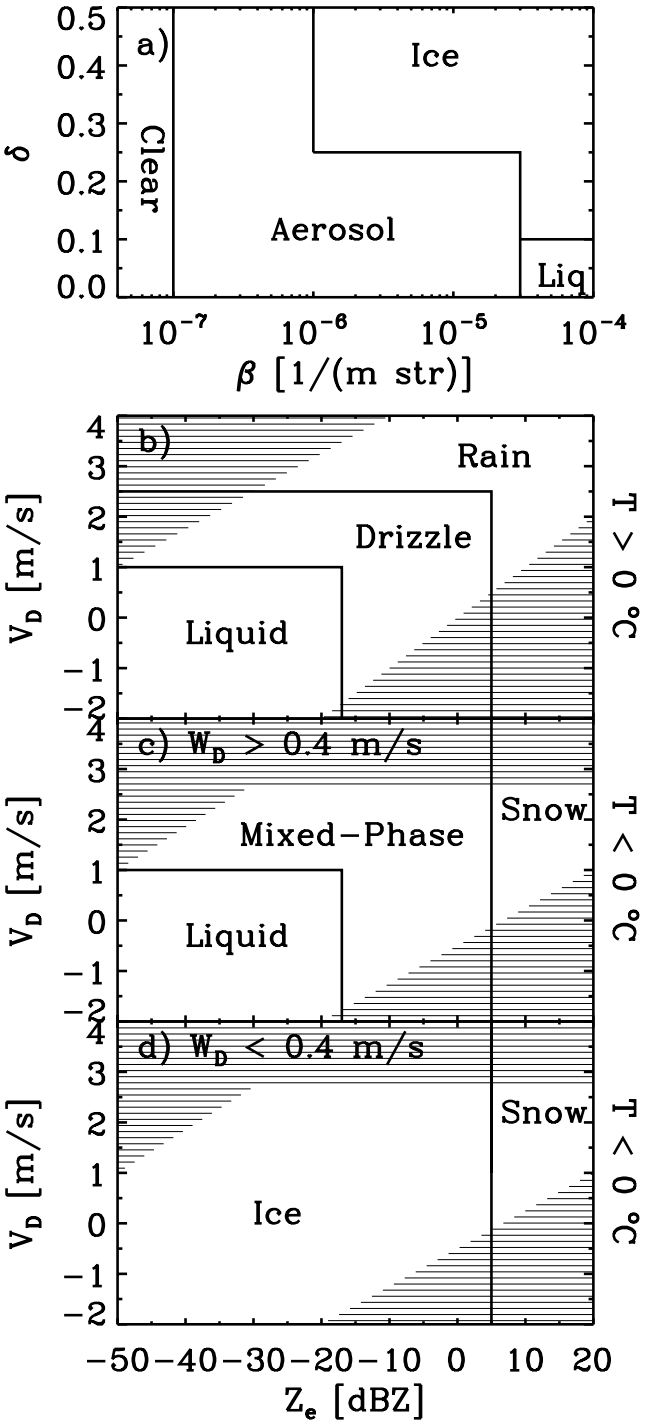

Figure 2. Classification diagrams. (a) The initial classification based on lidar backscatter and depolarization ratio measurements only. Radar measurements for the subset of data with (b) $T > 0°C$, (c) $T < 0°C$ and $W_D > 0.4$ m/s, and (d) $T < 0°C$ and $W_D < 0.4$ m/s. All radar panels contain shading in regions that do not often occur. All thresholds have been defined based on extensive experience with seven years of multisensor observations.

point of occultation. However, without supporting lidar measurements the radar may not correctly identify these cloud-top liquid layers. When radar identifies a cloud top no more than 750 m above the point of lidar occultation and $T < 0°C$, the scheme in Figure 2c is applied to distinguish liquid and mixed-phase clouds, regardless of spectrum width. This circumstance comes into play near the very top of the mid-level cloud just above the point of lidar occultation, where some regions have spectrum widths less than 0.4 m/s and would thus be classified as ice.

[17] At this point in the classification there is a full time-height cloud phase mask based solely on information from the lidar, radar, and temperature soundings which can be further constrained by other supporting measurements. First absolute temperature rules (step 5 in Table 2) can be applied which allow only ice or snow at $T < -40°C$ (the homogeneous freezing temperature) and only liquid phase hydrometeors at $T > 0°C$. In this case (Figure 1g), all clouds above 7 km (the height of $-40°C$) are ice phase.

[18] While the above constraint does not usually contribute much additional information, a LWP constraint (step 6) can significantly impact the classification. Due to the radiative significance of liquid water in Arctic clouds [e.g., *Shupe and Intrieri*, 2004], a LWP constraint of this fashion is imperative if the cloud classification product will contribute to computations of atmospheric radiation profiles. If LWP ≤ 0 g/m^2, indicating the absence of cloud liquid, and $T < 0°C$, all liquid-containing classifications in the vertical column are set to ice. On the contrary, if LWP is greater than the LWP retrieval uncertainty ($\sim$25 g/m^2 for a typical, two-channel MWR) indicating the presence of liquid water, but no liquid-containing class has been identified, a liquid layer must be specified. If a cloud base is identified by lidar, a liquid layer is classified immediately above that base, otherwise the liquid is assumed to start at the lowest observation height. The liquid layer depth extends up to an identified cloud top that is within 500 m or over a depth that provides an average liquid water content of 0.2 g/m^3.

[19] The final classification step (step 7 in Table 2) is a coherence filter which acts to decrease the pixilation, or speckle, in a classification and to apply some conditional rules. For each classified pixel, the surrounding 7×7 pixel box (in time-height space) is considered. If more than 35 of 49 pixels are classified as clear, then the central pixel is set to clear. If the central pixel is not set to clear and there are more than 7 of 49 pixels with the same type as the central pixel, it is left unchanged. Otherwise, the central pixel is set to the classification type that is most plentiful in the box. For each pixel, the filter is applied to the original unfiltered classification mask to negate the dependence on order. Some rules can also be applied to avoid certain erroneous classifications: 1) Thin (<200 m) ''ice'' layers directly above mixed-phase (or liquid) layers are reclassified as mixed-phase (or liquid); 2) drizzle classified above cloud liquid causes the liquid to be reclassified as drizzle; and 3) ice (or mixed-phase) classified above and below drizzle causes the drizzle to be reclassified as ice (or mixed-phase).

[20] Uncertainties in this classification method are related to the fixed thresholds specified in Figure 2 which in some cases might be better implemented in a probabilistic framework, to temperature variability that is not captured by

periodic radiosondes, and to the individual measurement uncertainties, particularly the estimate of LWP. At present there does not exist an independent cloud phase data set appropriate to validate these classifications. While frequent, unambiguous agreement regarding cloud phase among multiple instruments does act to verify the classifications, an objective quantification of the uncertainties is desired. This validation might be accomplished in the future using modeled clouds and instrument/measurement simulators.

4. Conclusions

[21] A cloud phase classification algorithm has been presented which provides a phase type for all clouds observed above an atmospheric observatory containing cloud radar, depolarization lidar, microwave radiometer, and radiosonde measurements. The algorithm combines information from these complementary measurements to identify cloud volumes by their phase components. Resulting classification masks can then be used to correctly apply cloud microphysics retrievals using remote sensors or to study the morphology of cloud types at a given location.

[22] The classifier introduced here has been specifically developed for observations of Arctic clouds. A similar approach could be applied to cloud observations at other locations, although detailed analysis of long data records and a thorough understanding of cloud measurements are required in order to determine the appropriate threshold parameters for the given location. Furthermore, although it employs multiple measurements, this classification might still be considered simplistic since it is based on fixed thresholds between parameters and cloud phase types. A logical extension of this method is to apply neural networks or fuzzy logic systems that are trained using these results. Such advances might further improve the classification for some of the borderline phase types such as warm mixed-phase cloud versus cold drizzle.

[23] **Acknowledgments.** This research was supported by the Office of Science (BER), U.S. Department of Energy, Grant DE-FG02-05ER63965 and the NOAA SEARCH Program. Thanks to Ed Eloranta and Taneil Uttal for supporting data and discussions.

References

Bankert, R. L. (1994), Cloud classification of AVHRR Imagery in maritime regions using a probabilistic neural network, *J. Appl. Meteorol.*, *33*, 909–918.

Baum, B. A., V. Tovinkere, J. Titlow, and R. M. Welch (1997), Automated cloud classification of global AVHRR data using a fuzzy logic approach, *J. Appl. Meteorol.*, *36*, 1519–1540.

Campbell, J. R., D. L. Hlavka, E. J. Welton, C. J. Flynn, D. D. Turner, J. D. Spinhirne, and V. S. Scott (2002), Full-time eye-safe cloud and aerosol lidar observations at atmospheric radiation measurement program sites: Instruments and data processing, *J. Atmos. Oceanic Technol.*, *19*, 431–442.

Crewell, S., and U. Lohnert (2003), Accuracy of cloud liquid water path from ground-based microwave radiometer: 2. Sensor accuracy and synergy, *Radio Sci.*, *38*(3), 8042, doi:10.1029/2002RS002634.

Duchon, C. E., and M. S. O'Malley (1999), Estimating cloud type from pyranometer observations, *J. Appl. Meteorol.*, *38*, 132–141.

Ebert, E. (1987), A pattern recognition technique for distinguishing surface and cloud types in the Polar regions, *J. Clim. Appl. Meteorol.*, *26*, 1412–1427.

Eloranta, E. W. (2005), High spectral resolution lidar, in *Lidar: Range-Resolved Optical Remote Sensing of the Atmosphere*, edited by K. Weitkamp, 455 pp., Springer-Verlag, New York.

Frisch, A. S., C. W. Fairall, and J. B. Snider (1995), Measurements of stratus cloud and drizzle parameters in ASTEX with a Ka-band Doppler radar and a microwave radiometer, *J. Atmos. Sci.*, *52*, 2788–2799.

Hu, Y.-X., D. Winker, P. Yang, B. Baum, L. Poole, and L. Vann (2001), Identification of cloud phase from PICASSO-CENA lidar depolarization: A multiple scattering sensitivity study, *J. Quant. Spectrosc. Radiat. Transfer*, *70*, 569–579.

Intrieri, J. M., M. D. Shupe, T. Uttal, and B. J. McCarty (2002), An annual cycle of Arctic cloud characteristics observed by radar and lidar at SHEBA, *J. Geophys. Res.*, *107*(C10), 8030, doi:10.1029/2000JC000423.

Liljegren, J. C., E. E. Clothiaux, G. G. Mace, S. Kato, and X. Dong (2001), A new retrieval for cloud liquid water path using a ground-based microwave radiometer and measurements of cloud temperature, *J. Geophys. Res.*, *106*, 14,485–14,500.

Luo, G., P. A. Davis, L. L. Stove, and E. P. McClain (1995), A pixel-scale algorithm of cloud type, layer, and amount for AVHRR data, part I: Nighttime, *J. Atmos. Oceanic Technol.*, *12*, 1013–1037.

Miller, S. W., and W. J. Emery (1997), An automated neural network cloud classifier for use over land and ocean surfaces, *J. Appl. Meteorol.*, *36*, 1346–1362.

Moran, K. P., B. E. Martner, M. J. Post, R. A. Kropfli, D. C. Welsh, and K. B. Widener (1998), An unattended cloud-profiling radar for use in climate research, *Bull. Am. Meteorol. Soc.*, *79*, 443–455.

Rossow, W. B., and R. A. Schiffer (1999), Advances in understanding clouds from ISCCP, *Bull. Am. Meteorol. Soc.*, *80*, 2261–2286.

Sassen, K. (1984), Deep orographic cloud structure and composition derived from comprehensive remote sensing measurements, *J. Clim. Appl. Meteorol.*, *23*, 568–582.

Shao, J. (2000), Fuzzy categorization of weather conditions for thermal mapping, *J. Appl. Meteorol.*, *39*, 1784–1790.

Shupe, M. D., and J. M. Intrieri (2004), Cloud radiative forcing of the Arctic surface: The influence of cloud properties, surface albedo, and solar zenith angle, *J. Clim.*, *17*, 616–628.

Shupe, M. D., P. Kollias, S. Y. Matrosov, and T. L. Schnieder (2004), Deriving mixed-phase cloud properties from Doppler radar spectra, *J. Atmos. Oceanic. Technol.*, *21*, 660–670.

Shupe, M. D., T. Uttal, and S. Y. Matrosov (2005), Arctic cloud microphysics retrievals from surface-based remote sensors at SHEBA, *J. Appl. Meteorol.*, *44*, 1544–1562.

Shupe, M. D., S. Y. Matrosov, and T. Uttal (2006), Arctic mixed-phase cloud properties derived from surface-based sensors at SHEBA, *J. Atmos. Sci.*, *63*, 697–711.

Talbot, L. M., B. G. Talbot, R. E. Peterson, H. D. Tolley, and H. D. Mecham (1999), Application of fuzzy grade-of-membership clustering to analysis of remote sensing data, *J. Clim.*, *12*, 200–219.

Tovinkere, V. R., M. Penaloza, A. Logar, R. C. Weger, T. A. Berendes, and R. M. Welch (1993), An intercomparison of artificial intelligence approaches for polar scene identification, *J. Geophys. Res.*, *98*, 5001–5016.

Turner, D. D. (2007), Improved ground-based liquid water path retrievals using a combined infrared and microwave approach, *J. Geophys. Res.*, *112*, D15204, doi:10.1029/2007JD008530.

Turner, D. D., S. A. Ackerman, B. A. Baum, H. E. Revercomb, and P. Yang (2003), Cloud phase determination using ground-based AERI observations at SHEBA, *J. Appl. Meteor.*, *42*(6), 701–715, doi:10.1175/1520-0450(2003)042<0701:CPDUGA>2.0.CO;2.

Turner, D. D., S. A. Clough, J. C. Liljegren, E. E. Clothiaux, K. Cady-Pereira, and K. L. Gaustad (2007), Retrieving liquid water path and precipitable water vapor from the Atmospheric Radiation Measurement (ARM) microwave radiometers, *IEEE Trans. Geosci. Remote Sens*, *45*, 3680–3690.

Wang, Z., and K. Sassen (2001), Cloud type and macrophysical property retrieval using multiple remote sensors, *J. Appl. Meteorol.*, *40*, 1665–1682.

Welch, R. M., S. K. Sengupta, A. K. Goroch, P. Rabindra, N. Rangaraj, and M. S. Navar (1992), Polar cloud and surface classification using AVHRR imagery: An intercomparison of methods, *J. Appl. Meteorol.*, *31*, 405–420.

Westwater, E. R., Y. Han, M. D. Shupe, and S. Y. Matrosov (2001), Analysis of integrated cloud liquid and precipitable water vapor retrievals from microwave radiometers during SHEBA, *J. Geophys. Res.*, *106*, 32,019–32,030.

M. D. Shupe, Cooperative Institute for Research in Environmental Science, University of Colorado, R/PSD3, 325 Broadway, Boulder, CO 80305, USA. (matthew.shupe@noaa.gov)